J Solid State Electrochem (1999) 3: 397–405 © Springer-Verlag 1999

ORIGINAL PAPER

Shalini Rodrigues · N. Munichandraiah · A.K. Shukla

AC impedance and state-of-charge analysis of a sealed lithium-ion rechargeable battery

Received: 23 September 1998 / Accepted: 22 February 1999

Abstract A 7.2 V, 1.25 Ah sealed lithium-ion rechargeable battery has been studied for estimating its state-of-charge (SOC) by AC impedance. The dispersion of impedance data over the frequency range between 100 kHz and 25 mHz comprises an inductive part and two capacitive parts. As the inductive behaviour of the battery is attributed to the porous nature of the electrodes, only the capacitive components have been examined. The data obtained at several SOC values of the battery have been analyzed by a non-linear least-squares fitting procedure. The presence of two depressed semicircles in the capacitive region of the Nyquist plots necessitated the use of an electrical equivalent circuit containing constant phase elements instead of capacitances. The impedance parameters corresponding to the low-frequency semicircle have been found useful for predicting the SOC of the battery, mainly because the magnitude of these parameters and their variations are more significant than those of the high-frequency semicircle. The frequency maximum (f_{max}) of the semicircle, the resistive component (Z') corresponding to f_{max}, the phase angle (ϕ) in the 5.0 Hz–0.1 Hz frequency range, the equivalent series resistance (R_s) and the equivalent series capacitance (C_s) have been identified as suitable parameters for predicting the SOC values of the lithium-ion battery.

Key words AC impedance · Lithium-ion battery · State-of-charge

S. Rodrigues · A.K. Shukla
Solid State and Structural Chemistry Unit,
Indian Institute of Science, Bangalore 560 012, India

N. Munichandraiah (✉)
Department of Inorganic and Physical Chemistry,
Indian Institute of Science, Bangalore 560 012, India
e-mail: muni@ipc.iisc.ernet.in
Tel.: +91-80-3092825
Fax: +91-80-3341683

Introduction

In a sealed lithium-ion rechargeable cell, both the anode (negative plate) and the cathode (positive plate) comprise intercalation materials with lattice structures into which guest species are intercalated and extracted topotactically, across a lithium-ion electrolyte of an aprotic solvent, without much structural modification of the host. The fully charged negative plate is made of lithiated carbon and has about the same electrochemical potential as metallic lithium. The discharged positive plate employs $LiCoO_2$, which develops a voltage of about 4 V with respect to lithium when it is fully charged. Both the volumetric and gravimetric energy densities of the lithium-ion batteries are at least twice the values for the present day lead-acid cells. Although the lithium-ion battery is the most advanced system among the various lithium-based batteries presently under development, the data on the characterization of the lithium-ion batteries are rather scanty in the literature owing to their sealed nature.

Among the various techniques employed for the characterization of sealed secondary batteries, alternating current (AC) impedance studies are known to provide several important parameters such as charge-transfer resistance, double-layer capacitance, etc. These parameters are seminal: (1) to derive information on the optimum utilization of the storage batteries, (2) to find the modes of the cell failures and (3) to determine the state-of-charge (SOC)[1].

The electrochemical impedance measurements of sealed batteries are rather difficult to analyze since the results obtained generally comprise lumped parameters of both the positive and negative electrodes. Furthermore, the separation of these lumped parameters into individual electrodes involves assumptions that are open to question. For example, in a recent study on a sealed

[1] SOC is the ratio of available capacity to the maximum attainable capacity

lithium-ion battery, galvanostatic transient data were analyzed and individual electrode parameters estimated assuming that the RC time constants of the individual electrodes were markedly different [1]. A direct estimation of these parameters is not accessible by non-destructive measurements since a suitable reference electrode cannot be introduced into sealed batteries. Because of these difficulties, only a few AC impedance studies on such batteries have been reported in the literature. In the present study, we have investigated the impedance behaviour of a commercially available sealed lithium-ion battery and have analyzed the data in the light of an equivalent-circuit model. The results have been used for predicting the SOC of the lithium-ion battery.

Phenomenology

When an electrochemical cell is excited by a low-amplitude AC signal, the output is generally out of phase owing to the presence of capacitive and rare inductive components of the cell. The measured total impedance constitutes the resistive and reactive components of the individual processes, which can be represented by an appropriate electrical analogue known as the electrical equivalent-circuit.

The electrical equivalent-circuit of a battery comprises the electrochemical processes occurring at the anode, the cathode and in the electrolyte, as shown in Fig. 1a. The significance of various circuit elements may be explained as follows. The battery electrodes are usually porous and the porosity of the electrodes leads to the impedance becoming inductive at high frequencies [2]. Therefore, L_a and L_c refer to inductors associated with the anode and the cathode, respectively. R_Ω refers to the ohmic resistance of the cell, which includes the resistances of the electrolyte, electrode base metal, electrode leads, terminals, etc. The charge-transfer resistances (R_a and R_c), the double-layer capacitances (C_a and C_c) and the Warburg impedances (W_a and W_c) of the respective anode and the cathode are included in the circuit following Randles' equivalent-circuit model.

The charge-transfer resistance (R_a or R_c) of an electrochemical process is related to the exchange current ($I_{o,a}$ or $I_{o,c}$) as:

$$R_a = RT/n_aFI_{o,a} \quad (1)$$

and the Warburg impedance (W_a or W_b) is defined as:

$$W_a = \sigma_a\omega^{-1/2} - j\sigma_a\omega^{-1/2} \quad (2)$$

where n is the number of electrons and σ is the Warburg coefficient, which is related to the diffusion coefficient and the concentrations of the species involved in the reaction. Subscripts a and c refer to the anode and cathode, respectively. As R_a (or R_b) and σ_a (or σ_b) are related to the concentrations, it follows that these parameters and hence the total impedance of the battery would vary with its SOC.

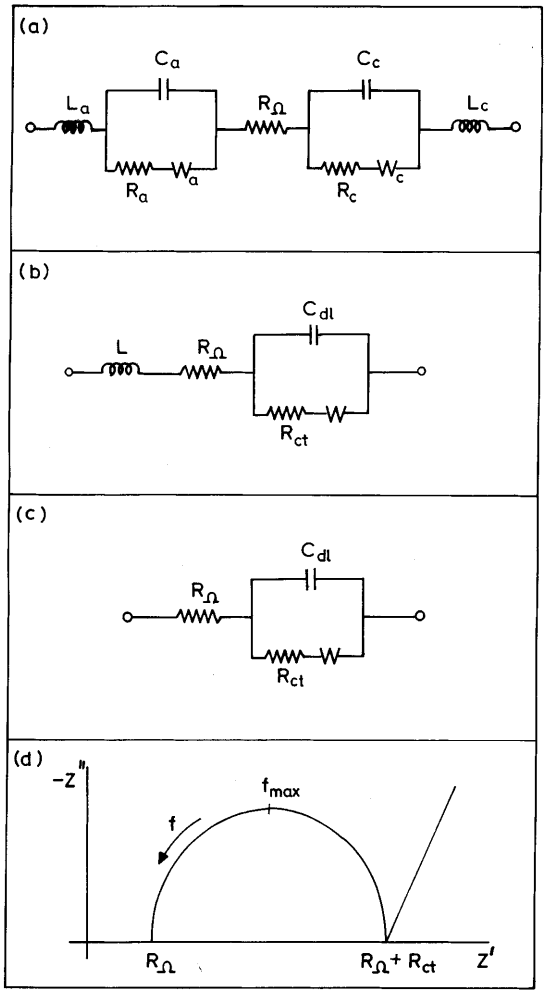

Fig. 1 **a** Equivalent circuit of a two-terminal energy storage cell with individual electrode parameters. L, C, R and W refer to inductance, double-layer capacitance, charge-transfer resistance and Warburg impedance, respectively. Subscripts a and c refer to the anode and cathode. R_Ω is the ohmic resistance. **b** Equivalent circuit with lumped parameters of the cell. R_{ct}, C_{dl} and W refer to charge-transfer resistance, double-layer capacitance and Warburg impedance of the battery respectively. **c** Equivalent circuit same as in **b** but without inductance. **d** A schematic complex plane impedance spectrum corresponding to the equivalent circuit shown in **c**

A semicircle on a complex-plane diagram (i.e. imaginary part, Z'' vs. real part Z') indicates the presence of a parallel combination of a resistor and a capacitor if Z'' is negative, or a parallel combination of a resistor and an inductor if Z'' is positive. For an equivalent circuit of a two-terminal storage battery (Fig. 1), it follows that the inductive, capacitive and linear distribution of the spectrum characterizing separately the anode and the cathode of the battery is expected. One may observe this in an experimental spectrum, provided the magnitude of the parameters and time constants (RC) corresponding to the anode and the cathode differ appreciably. In general, the total resistance of an energy storage cell is

less than an ohm, and the parameters of the anode and the cathode are comparable in magnitude. As a result, the impedance spectrum may not clearly resolve corresponding to the individual electrode parameters, but it may represent the cell as a whole. The equivalent circuit may, therefore, be reduced as shown in Fig. 1b [3]. The lumped parameters of the whole cell are shown in Fig. 1b. As the inductance offers reactance at high AC frequencies, and if the experiments are carried out at low frequencies, the contribution of the impedance by the inductance becomes negligibly small. Under these conditions, the inductance (L) may be ommitted from Fig. 1b and the equivalent circuit further reduces to the one shown in Fig. 1c. The complex-plane diagram of the impedance spectrum corresponding to the simplified equivalent circuit contains a semicircle and a linear spike as shown in Fig. 1d. The high-frequency intercept of the semicircle provides the value of R_Ω and the low-frequency intercept gives the value of charge-transfer resistance, R_{ct}. The double-layer capacitance (C_{dl}) can be obtained from the AC frequency corresponding to the maximum on the semicircle (f_{max}) as:

$$C_{dl} = 1/(2\pi f_{max} R_{ct}) \quad (3)$$

Experimental

Sealed lithium-ion rechargeable batteries (Sony Model NP-510) were employed for the present study. The nominal voltage of the battery with two cells of each 4.2 V connected in series is 8.4 V. The constituents of each cell are represented as: LiC/PC + DMC + $LiPF_6$ (1 M)/$Li_{1-x}CoO_2$. The battery is specified to deliver a capacity of 1.25 Ah at $C/5$ rate. The suggested operating voltage range of the battery is 6.0–8.4 V. The battery was subjected to a few charge/discharge cycles to ensure the reproducibility of its discharge capacity prior to the present investigations. The battery delivered a discharge capacity of 1.10 Ah at $C/5$ rate. AC impedance measurements of the lithium-ion battery at several SOC values were carried out by an electrochemical impedance analyzer (EG&G PARC model 6310). The cell was charged to the required SOC at $C/5$ rate and allowed to stand for 3 h under open-circuit conditions prior to the measurements. It was excited by an AC signal of 5 mV at the open-circuit voltage and impedance measurements were made in the frequency range 100 kHz–25 mHz. As the instrument had a voltage limitation, the measurements could be made at cell voltages below 8.0 V. The SOC $\sim$ 0.7 corresponded to 8.0 V of the battery. DC polarization studies of the battery were also carried out by a potentiostat/galvanostat (EG&G model Versastat). The battery was subjected to a linear voltage sweep at a scan rate of 0.1 mV s^{-1} in the voltage range $\pm$5 mV of the open-circuit voltage. All experiments were conducted at 19 $\pm$ 1 °C.

Results and discussion

The impedance spectrum of the lithium-ion battery at SOC $\sim$ 0 is shown as Nyquist and Bode plots in Fig. 2. The Nyquist plot (Fig. 2a) comprises an inductive distribution of the data at frequencies >1.259 kHz followed by two capacitive semicircles in the 1.259 kHz–25 mHz frequency range. The phase angle (ϕ) versus AC frequency plot (Fig. 2b) suggests the value of ϕ to be positive at high frequencies, corresponding to the inductive behaviour of the battery. The phase angle gradually becomes negative and reaches the peak value at −24°, reflecting the capacitive behaviour of the battery in frequency range 1.259 kHz–25 mHz. By an extrapolation of the modulus of impedance ($|Z|$) in the low-frequency region, a total cell resistance (R_T) of 1.09 Ω is obtained (Fig. 2b).

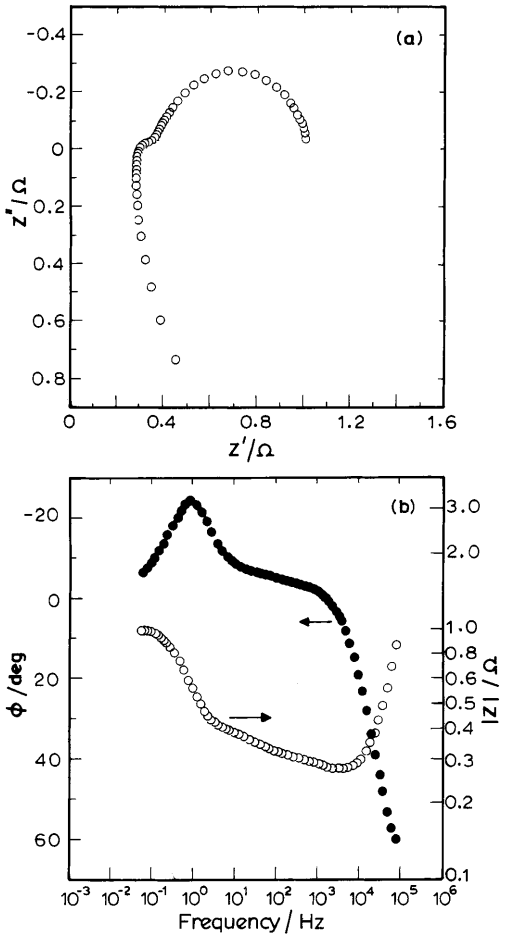

Fig. 2 Impedance spectrum of a lithium-ion battery at SOC ≈ 0, represented in a Nyquist plot (**a**) and a Bode plot (**b**). Z', Z'', $|Z|$ and ϕ refer to the real component, imaginary component, modulus of impedance and phase angle, respectively

The impedance parameters of the lithium-ion battery were evaluated from the experimental impedance spectrum by an equivalent circuit non-linear least squares (NLLS) fitting procedure due to Boukamp [4]. The equivalent circuit, which gave the values of the parameters to fit the experimental data satisfactorily, is shown in Fig. 3. Various circuit elements shown in Fig. 3 are explained as follows. The high-frequency impedance data are inductive in the form of a semicircle (Fig. 2). Therefore, the inductance (L) and a resistance (R_L) are taken in parallel. The element R_Ω represents the ohmic resistance of the cell. The two capacitive semicircles are

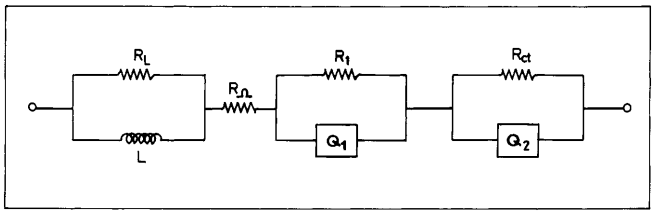

Fig. 3 Equivalent circuit used for NLLS fitting of the experimental data of the lithium-ion battery

depressed, more so in case of the high-frequency small semicircle. Hence, a constant phase element (CPE) denoted as Q_1 is taken in parallel to a resistance R_1 corresponding to the high-frequency semicircle. The CPE arises due to distribution of microscopic material properties. The interfaces between the electrode/electrolyte of the Li-ion cell are not smooth and uniform, as the electrodes are made using fine particles of the active materials. The intercalation and deintercalation of lithium processes are not uniform throughout the surface of the electrodes. Reaction resistance and capacitance contribution may differ with the electrode position, non-uniform thickness of the electrode materials, etc. Owing to these distributions, the semicircles of the Nyquist plots are depressed. The admittance representation of CPE is given as [4]:

$$Y^* = Y_0(j\omega)^n \tag{4}$$

where Y_0 is an adjustable parameter and $\omega = 2\pi f$. For $n = 0$, CPE represents a resistance, $R(=Y_0^{-1})$; for $n = 1$, a capacitance, $C(=Y_0)$; for $n = 0.5$, a Warburg impedance; and for $n = -1$, an inductance $L(=Y_0^{-1})$. The NLLS-fit technique was employed using the equivalent circuit (Fig. 3) with the circuit description code (CDC) [4]: $(RL)R(RQ)(RQ)$. The elements within a set of parentheses denote their parallel combination, while the elements out of parentheses denote a series combination. The starting values were obtained from the Data Cruncher subprogram prior to using the values in the NLLS-fit program. A similar procedure has been successfully employed to analyze the impedance of Li/solid polymer electrolyte/Li symmetrical cells [5]. The values of the parameters obtained for the data shown in Fig. 2 for SOC $\approx$ 0 and other SOC values are given in Table 1.

Table 1 Impedance parameters of the lithium-ion battery

	SOC							
	0	0.09	0.14	0.28	0.34	0.42	0.56	0.70
Voltage (V)	6.09	6.38	6.73	7.25	7.39	7.57	7.81	7.94
R_L (Ω)	3.19	3.22	3.40	3.41	3.35	3.30	3.16	3.26
L (μH)	1.55	1.60	1.62	1.66	1.65	1.64	1.59	1.61
R_Ω (Ω)	0.27	0.27	0.26	0.26	0.25	0.25	0.25	0.25
R_1 (Ω)	0.13	0.14	0.14	0.22	0.26	0.24	0.21	0.21
Q_1 (Ω^{-1})	0.34	0.42	0.58	1.11	1.30	1.21	1.10	1.02
n_1	0.53	0.48	0.45	0.37	0.34	0.36	0.38	0.39
R_{ct} (Ω)	0.62	0.55	0.45	0.35	0.31	0.29	0.27	0.26
Q_2 (Ω^{-1})	0.62	0.62	0.61	0.65	0.65	0.66	0.65	0.65
n_2	0.91	0.93	0.95	1.00	1.00	1.00	1.00	1.00

The impedance plots consisting of the experimental data points and the curves simulated from the fit parameters are shown in Fig. 4. It is seen that there is a good agreement between the experimental and simulated data in all the impedance representations.

The inductance behaviour of electrochemical power sources has been reported and reviewed in the literature [2]. Gutmann [6], from his studies on Zn-MnO_2 dry cells, reported that these systems exhibit lagging currents. In order to explain this behaviour, a pseudo-inductance, defined as the capability of a space to store electrical energy reversibly and kinetically, was proposed. The kinetic process was ascribed to the visco-elastic behaviour exhibited at higher frequencies and/or in higher viscous systems. Keddam et al. [7] reported inductive behaviour of Pb-acid batteries at high frequencies. The value of the self-inductance was nearly invariant with the SOC of the battery, which was equal to about 1 μH and schematically shunted to a parallel resistance of about 0.6 Ω. The inductance behaviour was attributed to the geometrical nature of conductors and electrodes, and not to the faradaic processes in the battery. It is thus clear that the inductive distribution of the impedance of the lithium-ion battery is due to the porous nature of the electrodes.

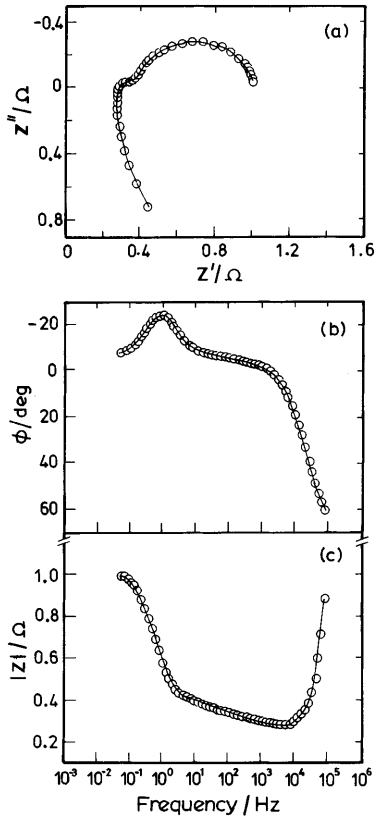

Fig. 4 Impedance spectrum of the lithium-ion battery shown as Nyquist (**a**), Bode ϕ (**b**) and Bode $|Z|$ (**c**) plots. The *continuous lines* are simulated from NLLS fit results and the points are the experimental data

The lithium-ion battery employed during this study consists of a lithiated graphite negative electrode and a lithium cobalt oxide positive electrode, which are made of fine particles mixed with conducting carbon powders and polymer binders [8]. Hence, both the electrodes are expected to be highly porous. Besides, both the electrode materials are insertion compounds in which Li^+ ions undergo reversible intercalation and deintercalation during charge/discharge cycles. Such a nature of the electrodes may be treated as microporous. In analogy to the results of Keddam et al. [7], the value of the inductance of the lithium-ion battery was obtained to be about 1.5 μH shunted by a parallel resistance of about 3.19 Ω (Table 1). A summation of all resistance values of the battery at SOC $\sim$ 0 in Table 1 results in a value of about 4.19 Ω which, in principle, should be equal to the DC resistance of the battery. To cross-examine these data, the cell resistance was also measured using slow voltage sweep DC voltammetry. The value of total cell resistance thus obtained was about 1 Ω, which is comparable to the sum of R_Ω, R_1 and R_{ct} in Table 1. Similar total cell resistance values have been reported by a galvanostatic transient study [1]. Thus, it followed that the shunting resistance (R_L) across the inductance (Fig. 3) was only schematic, and is an artifact of the fitting procedure. The values of the inductance (L) and the shunting resistance (R_L) are, therefore, considered irrelevant for characterizing the battery and these parameters are omitted during subsequent discussion. The fitting procedure was repeated after excluding the inductive dispersion of the impedance data and, L and R_L in the equivalent circuit. Values of the rest of the parameters remained unaltered. It was thus confirmed that the inductance data did not influence the rest of the impedance spectrum.

The resistance R_Ω is ascribed to the ohmic resistance of the battery, which includes the resistance of the electrolyte, current collectors, battery terminals, intercell connectors, etc. The values of R_Ω obtained from the NLLS fit as well as from the high-frequency intercept of the Nyquist plot are nearly similar (Table 1) for SOC $\sim$ 0 of the lithium-ion battery. In the literature, there is a contradiction regarding the assignment of the capacitive semicircles to the respective electrodes of the battery. In recent studies of comparative evaluation of different cathode materials, Ozawa [8] has reported AC impedance of a lithium-ion system consisting of carbon and $LiCoO_2$. Similar to the present results, the complex-plane plot of the impedance spectrum contained two semicircles of different sizes, the high-frequency semicircle being smaller than that for the low frequency. It was found that the impedance plots obtained by using a cell with only a fully charged carbon electrode was similar to the larger semicircle at low frequencies. Based on these observations, the low-frequency larger semicircle was attributed to the charge-transfer reaction at the carbon electrode and the high-frequency smaller semicircle to the charge-transfer reaction at $LiCoO_2$ electrode. Similar explanations for impedance results were reported by Isaacson et al. [9] and Braatz et al. [10]. A study of the literature, however, suggested that the impedance data of the $LiCoO_2$ electrode alone contained two semicircles. Thomas et al. [11] invoked two different physical processes to account for the semicircle which was present in addition to Randles' equivalent circuit, namely (1) adsorption of Li^+ ions or propylene carbonate solvent molecules onto the surface of the electrode without charge transfer, and (2) formation of an ionically conducting but electronically insulating surface layer at the electrode surface. By a systematic analysis of various equivalent circuits representing the above two processes, it was concluded that the latter process, viz. formation of a surface layer on $LiCoO_2$ electrode, was responsible for the additional high-frequency smaller semicircle. In a similar single-electrode study with $LiNiO_2$, $LiCoO_2$ and $LiMn_2O_4$ electrodes in non-aqueous media, Aurbach et al. [12] reported a pair of semicircles of unequal size. The high-frequency smaller semicircle was attributed to the formation of a Li_2CO_3 surface layer and the low-frequency larger semicircle to the charge-transfer reaction. In the case of a lithiated graphite electrode, a single semicircle followed by a linear spike was reported [12].

From the foregoing, it is clear that the pair of semicircles observed in the impedance spectrum of the lithium-ion battery may not be easily resolved for the purpose of assigning to individual electrodes. As the kinetics of both the electrode reactions are also similar in magnitude, which are characterized by very low charge-transfer resistances, it is probable that the RC time constants of the anode and the cathode processes are similar in magnitude. In such a situation, the low-frequency larger semicircle may be attributed to a combined equivalent circuit comprising both the electrodes, and the high-frequency smaller semicircle to a passive layer on the cathode, or on both the electrodes.

The impedance spectra recorded at different SOC values of the lithium-ion battery after omitting the inductive distribution are shown in Fig. 5. The inductive

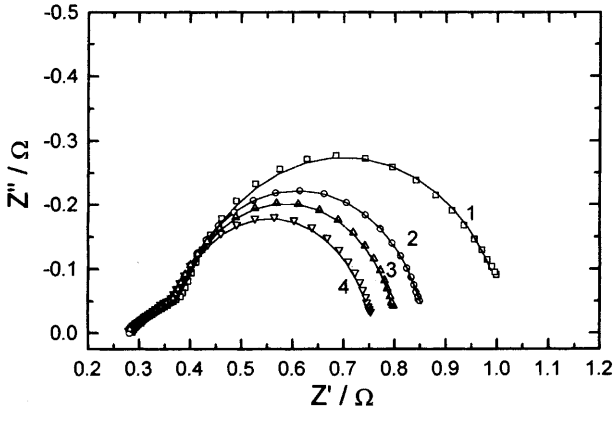

Fig. 5 Impedance spectra of the lithium-ion battery at SOC $\approx$ 0 (*1*), 0.14 (*2*), 0.28 (*3*), 0.42 (*4*). The inductive data are omitted. Experimental data are shown by *symbols* and theoretical data are shown by *solid lines*

distribution of the impedance occurred at frequencies >1.26 kHz for all SOC values of the battery. It is seen that the size of the low-frequency semicircle decreases with an increase in SOC, whereas the changes in the high-frequency semicircle are not clearly noticeable. The battery voltage and the impedance parameters are shown against the SOC of the battery in Figs. 6–8. It is seen that the battery voltage increases with an increase in its SOC (Fig. 6a). Although the increase of battery voltage is asymptotic, the curve has a higher slope in the low SOC region than in the high SOC region. The voltage may be an appropriate parameter to monitor the SOC of the battery to some extent. The ohmic resistance (R_Ω) decreases asymptotically from 0.27 Ω at SOC ≈ 0 to about 0.25 Ω at SOC ≈ 0.7 (Fig. 6b). As the decrease in magnitude of R_Ω is very small and the major part of the decrease lies between SOC ≈ 0 and 0.3, its usefulness to predict the SOC is limited. Analogous to R_Ω, the change in magnitude of R_1 (resistance of the surface film) is also very low and varies from 0.12 Ω at SOC ≈ 0 to about 0.20 Ω at SOC ≈ 0.7 (Fig. 6c). Contrary to R_Ω, which decreases with an increase of SOC, R_1 is found to increase. Both the increase in R_1 and the decrease in R_Ω with SOC may be explained on the basis of surface film formation. The surface film grows thicker on the positive electrode with an increase of the SOC and, thus, its resistance increases (Fig. 6c). Since propylene carbonate or ethylene carbonate solvent molecules are used up for the growth of the surface film, there is a loss in the quantity of solvent, which leads to an increase in the concentration of Li^+ ions in the electrolyte. It is therefore likely that the conductivity of the electrolyte increases with the concomitant decrease in R_Ω.

The magnitude of R_{ct} (charge-transfer resistance) decreases with an increase in the SOC (Fig. 6d). Although the decrease in R_{ct} is non-linear, the magnitude of the decrease is quite significant from 0.62 Ω at SOC ≈ 0 to 0.27 Ω at SOC ≈ 0.7. Of the three resistive components, R_{ct} appears to be the most appropriate parameter to predict the SOC of the battery, but for its non-linear variance. The values of R_{ct} are appreciably higher than the values of R_Ω and R_1, and the contribution of R_{ct} is significant with a concomitant decrease in the total battery resistance with an increase in the SOC.

The values of the constant phase elements, Q_1 and Q_2, also vary with the SOC, as shown in Fig. 7. The value of the coefficient n_1 corresponding to Q_1 varies around 0.5 (Fig. 8a), thus suggesting Warburg behaviour of the high-frequency semicircle. The value of the

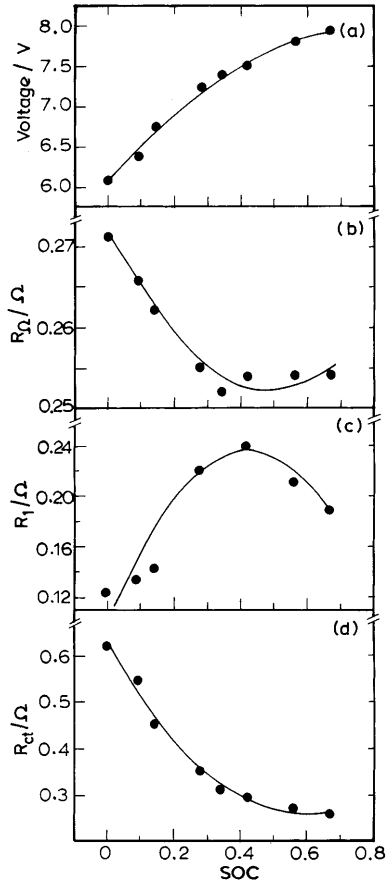

Fig. 6 Dependence of battery voltage (**a**), resistive component R_Ω (**b**), R_1 (**c**) and R_{ct} (**d**) at various SOC values of the lithium-ion battery

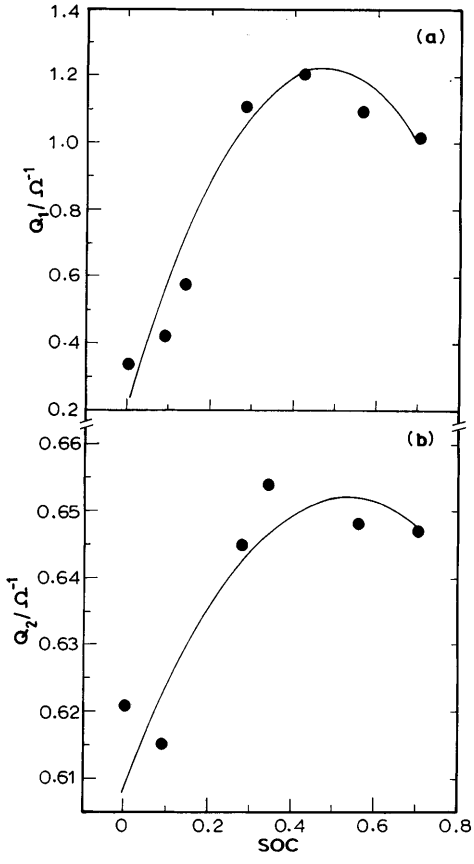

Fig. 7 Dependence of the constant phase element (CPE) Q_1 (**a**), and Q_2 (**b**) on the SOC values of the battery

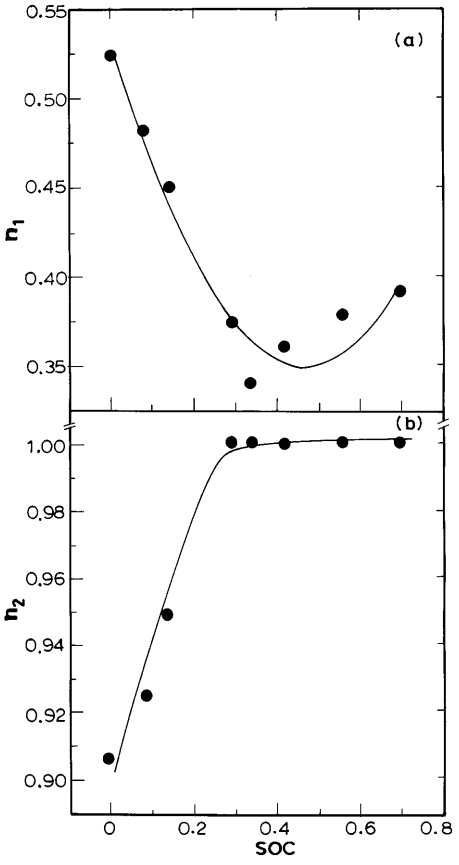

Fig. 8 Dependence of the coefficient of the constant phase element n_1 (**a**) and n_2 (**b**) on the SOC values of the battery

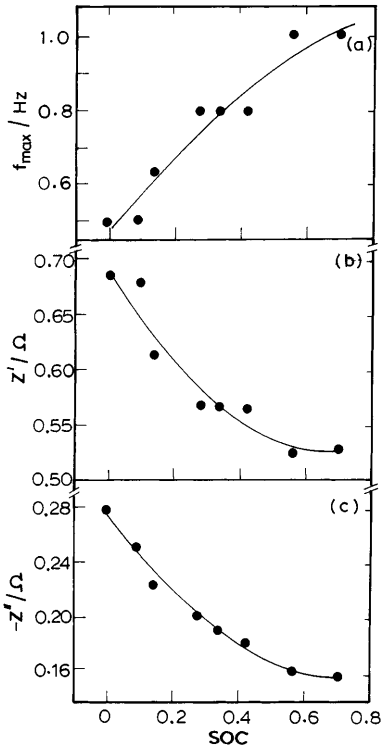

Fig. 9 Dependence of frequency maximum (f_{max}) (**a**), Z' (**b**) and Z'' (**c**) corresponding to f_{max} on the SOC values of the battery

coefficient n_2 corresponding to Q_2, however, is close to unity (Fig. 8b); the corresponding CPE is therefore likely to be capacitive in nature. The low-frequency large semicircle was evaluated to obtain the double-layer capacitance (C_{dl}) using Eq. (3), and it was found that C_{dl} was close to Q_2.

From the foregoing, it follows that the impedance parameters depend on the SOC of the lithium-ion battery. The variations in the magnitude of these parameters, however, are generally non-linear. In order to identify suitable parameters, other than those discussed above, which show strong dependence on the SOC, the low-frequency semicircle was employed. The values of f_{max} and the corresponding Z' and $Z''$are plotted against the SOC in Fig. 9; the values of the phase angle (ϕ) at several frequencies are plotted in Fig. 10. It is seen that f_{max} increases from about 0.5 Hz at SOC $\approx$ 0 to about 1.0 Hz at SOC $\approx$ 0.7 (Fig. 9a). On the other hand, Z' and Z'' corresponding to the f_{max} decrease in magnitude with an increase of SOC (Fig. 9b and c). The decrease in magnitude of Z'', however, is smaller compared to Z'. A significant decrease in the value of Z' from about 0.7 Ω at SOC $\approx$ 0 to about 0.5 Ω at SOC $\approx$ 0.7 could be used to predict the SOC of the lithium-ion battery. An examination of Fig. 10 suggests that ϕ varies significantly with the SOC of the battery at 0.5 Hz. The ϕ value

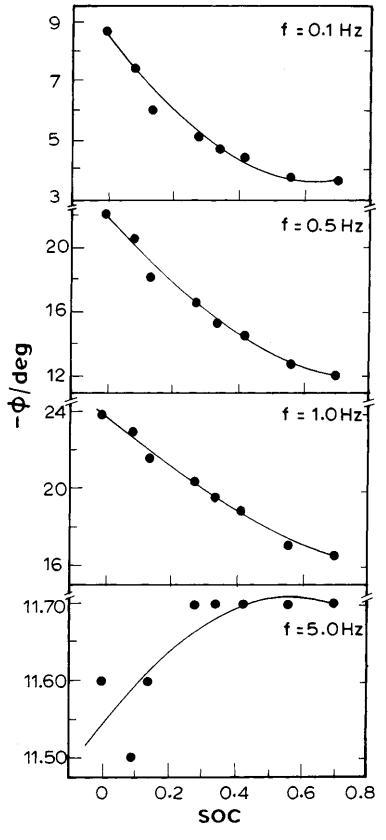

Fig. 10 Dependence of phase angle (ϕ) on SOC values of the battery at different frequency (f) values

decreases from 22° at SOC ≈ 0 to about 12° at SOC ≈ 0.7 at 0.5 Hz. Also, at 1 Hz, ϕ decreases from about 24° at SOC ≈ 0 to about 16° at SOC ≈ 0.7. At frequencies of 0.1 Hz and 5 Hz, however, the magnitude of ϕ is very low and there is no significant variation in its value with SOC. It is thus clear that ϕ is also useful for predicting the SOC of the lithium-ion battery at a frequency value between 0.5 Hz and 1.0 Hz.

Equivalent series (or parallel) resistance and capacitance have been reported for prediction of the SOC of batteries [13, 14]. Such an approach was also adopted in the present study. The low-frequency larger semicircle (Fig. 2) resulted from a parallel combination of charge-transfer resistance (R_{ct}) and double-layer capacitance ($C_{dl} \simeq Q_2$), as discussed earlier. The total impedance arising out of R_{ct} and C_{dl} could be transformed into a series combination of a resistance and a capacitance. The equivalent series resistance (R_s) and the equivalent series capacitance (C_s) may be calculated from R_{ct} and C_{dl} using the following expressions:

$$R_s = R_{ct}/(1 + (\omega R_{ct} C_{dl})^2) \quad (5)$$

and

$$C_s = C_{dl}(1 + 1/(\omega R_{ct} C_{dl})^2) \quad (6)$$

The values of R_s and C_s were calculated for several frequencies ranging between 5 Hz and 25 mHz, encompassing the low-frequency semicircle. It was found that the R_s values obtained were invariant at any SOC for all frequencies < 0.1 Hz (Fig. 11a). There is a decrease in the R_s value from about 0.62 Ω at SOC ≈ 0 to about 0.25 Ω at SOC ≈ 0.7. At frequencies higher than 0.1 Hz, the R_s values and its variation with SOC are insignificant. Unlike the magnitude of R_s, the magnitude of C_s is found to be higher, in particular at lower frequencies (Fig. 11b). At 25 mHz, the value of C_s is about 200 F at SOC ≈ 0 and increases to about 900 F at SOC ≈ 0.7. Although the magnitude is lesser at frequencies > 25 mHz, C_s is found to increase significantly with the SOC. Therefore the equivalent series capacitance (C_s) is an appropriate parameter to monitor the SOC of the lithium-ion battery, in particular at lower frequencies.

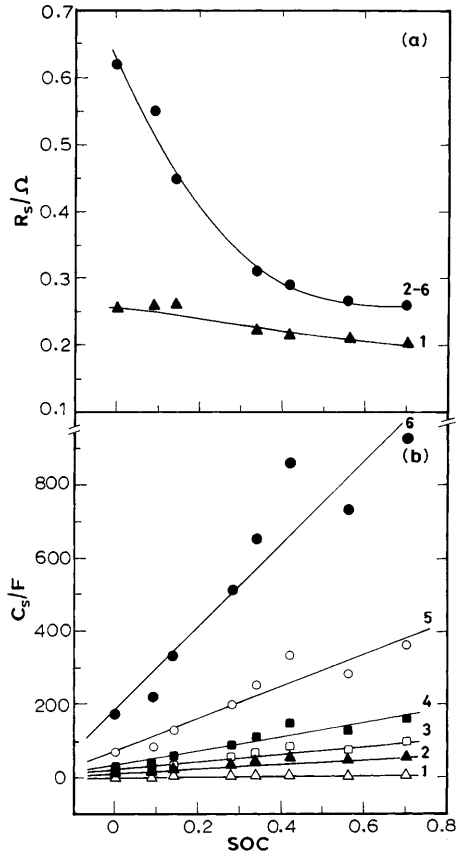

Fig. 11 Dependence of equivalent series resistance R_s (**a**) and equivalent series capacitance C_s (**b**) SOC values of the battery at frequency (Hz) values of 0.5 (*1*), 0.1 (*2*), 0.08 (*3*), 0.06 (*4*), 0.04 (*5*) and 0.025 (*6*)

Conclusion

The present study suggests that the AC impedance spectrum of the lithium-ion battery comprises an inductive part and two capacitive components in the frequency range 100 kHz–25 mHz. The impedance parameters of the battery were obtained by a NLLS procedure. Although the battery impedance could be measured only up to the SOC value of 0.7 and the impedance parameters could not be separated for the individual electrodes, the parameters of the larger semicircle of the Nyquist representation have been found to be useful for predicting the SOC of the battery. In particular, the equivalent series capacitance (C_s) shows a large variation from about 200 F at SOC ≈ 0 to about 900 F at SOC ≈ 0.7. The impedance parameters derived from the second semicircle are helpful in predicting the SOC of the battery.

Acknowledgements Financial support from IISc-ISRO Space Technology Cell is gratefully acknowledged.

References

1. Ganesh Kumar V, Munichandraiah N, Shukla AK (1997) J Appl Electrochem 27: 43
2. Hampson NA, Karunathilaka SAGR, Leek R (1980) J Appl Electrochem 10: 3
3. Sathyanarayana S, Venugopalan S, Gopikanth ML (1978) J Appl Electrochem 8: 479
4. Boukamp BA (1989) Equivalent circuit, users manual. University of Twente, The Netherlands
5. Munichandraiah N, Scanlon LG, Marsh RA (1998) J Power Sources 72: 203
6. Gutmann F (1965) J Electrochem Soc 112: 94
7. Keddam M, Stoynov Z, Takenouti H (1977) J Appl Electrochem 7: 539
8. Ozawa K (1998) Solid State Ionics 69: 212

9. Isaacson MJ, Daman ME, Hollandsworth RP (1977) In: Cairns EJ, McLarnon F (eds) Proceedings of the thirty second intersociety energy conversion engineering conference. American Institute of Chemical Engineers, New York, p 31
10. Braatz PO, Lim KC, Lackner AM, Smith WH Jr, Margerum JD, Lim HS (1997) Abstracts of joint international meeting on batteries & fuel cells for portable applications and electric vehicles. The Electrochemical Society, Pennington, NJ, p 134
11. Thomas MGSR, Bruce PG, Goodenough JB (1985) J Electrochem Soc 132: 1521
12. Aurbach D, Levi MD, Levi E, Schechter A (1997) Abstracts of the joint international meeting on batteries & fuel cells for portable applications and electric vehicles. The Electrochemical Society, Pennington, NJ, p 124
13. Sathyanarayana S, Venugopalan S, Gopikanth ML (1979) J Appl Electrochem 9: 125
14. Viswanathan VV, Salkind AJ, Kelley JJ, Ockerman JB (1995) J Appl Electrochem 25: 716